Journal of Materials Science: Materials in Electronics (2019) 30:9623–9633
https://doi.org/10.1007/s10854-019-01296-y

# Photocatalytic performance of $TiO_2$@$SiO_2$ nanocomposites for the treatment of different organic dyes

Shimaa Nabih[1] · Ahmed Esmail Shalan[2] · Esraa Samy Abu Serea[3] · Mona A. Goda[1,4] · Mohamed Fathi Sanad[5]

Received: 11 December 2018 / Accepted: 8 April 2019 / Published online: 12 April 2019


**Abstract**
Photocatalytic degradation of pollutant using $TiO_2$@$SiO_2$ nanocomposites (NCs) is a well route for the treatment of the organic waste in aquatic life. The recent work focuses on the removal of many organic dyes like methylene blue, eosin and safranin and study the pollutant degradation of them using the activity and high efficiency of titania as well as nanostructured titania@silica. The impregnation of silica with anatase-type $TiO_2$ was carried out through a sol–gel way. The obtained powders were checked and characterized using $N_2$ adsorption–desorption complete isotherm at low temperature, BET, FESEM, XRD, PL, UV–Vis spectroscopy, diffuse reflectance spectra and the photocatalytic activity to attain the homogeneity distribution of the nanostructure particles inside the matrix. $TiO_2$@$SiO_2$ material displayed good photocatalytic properties compared to a pure titania. Different parameters as the type of the photocatalyst, pH of solution, amount of the photocatalyst and adsorption were studied. In addition, reusability for dye removal under consecutive cycles was also investigated. Photocatalytic activity and the excellent properties of the $TiO_2$@$SiO_2$ NCs displayed that these materials can consider being good candidate considered in water treatment applications.

## 1 Introduction

Oxidative degradation of unlimited amount of organic pollutants from wastewater is a worthy significant research field [1–5]. Different industrial chemical processes like purification of water and removing of toxic materials as well as organic residues have been obtained by photocatalytic oxidations [6–11]. Photocatalyst powder materials are mainly used for pollutant degradation process [12–14]. Excitation of electrons between levels of $TiO_2$ nanoparticles through the irradiation in the UV region may cause pollutant degradation via environmental-friendly system. After the electrons exited from valence band (VB) to conduction band (CB), a strong oxidant matter can produce by the reaction of the existing holes founded in the VB with hydroxyl group, which in turn oxidizes an adsorbed organic pollutant to obtain nontoxic products [15–17]. Semiconductors materials are good candidates for wastewater treatment through a photocatalysis reaction [18–20]. Organic materials are popular pollutants in wastewaters that may originate from different industries. Degradation of organic molecules by advanced oxidation processes using wide spectrum of semiconductors has recently been documented [21–23]. One can notice plainly that titania is auspicious photocatalyst to remove different types of toxic molecules using photocatalytic process because of its high stability composition [24], strong oxidizing power [25] and low cost of the precursors [26]. However, low surface area and rapid charge recombination were the main causes for the industrialization limitation of some semiconductors used [27, 28]. Incorporation of noble metal to different metal oxide surface improves the photocatalytic reactivity to get rid of the organic pollutants through improving the electron separation, and this

Shimaa Nabih and Ahmed Esmail Shalan have contributed equally to this work.

✉ Ahmed Esmail Shalan
a.shalan133@gmail.com; a.shalan@cmrdi.sci.eg

[1] Basic Science Department, Modern Academy for Engineering and Technology, Maadi, Egypt

[2] Advanced Materials Division, Electronic & Magnetic Materials Department, Central Metallurgical Research and Development Institute (CMRDI), Helwan, Cairo 11421, Egypt

[3] Chemistry & Biochemistry Department, Faculty of Science, Cairo University, Cairo, Egypt

[4] Chemistry Department, Faculty of Science, Cairo University, Cairo, Egypt

[5] Basic Science Department, British University in Egypt, Misr-Ismailia Road, El-Sherouk City, Cairo 11837, Egypt

type of modifications was recently investigated [29, 30]. However, the cost was very high, we modify a new trend for using the high adsorption power of silica ($SiO_2$) to add more stability and reactivity instead of using transition metals and lowering the total cost of the operation. Herein, we use easy method to load titania over silica nanoparticles in presence of CTAB as pore directing agent to form $TiO_2$@$SiO_2$ nanocomposites. Different techniques were applied to characterize the prepared materials, which include; complete isotherm (BET), HRTEM, UV–Vis spectroscopy and XRD. These instruments were used to provide information about morphology, crystal structures, optical properties and photocatalytic activity for the obtained samples. Terephthalic acid probing technique was incorporated to confirm the effect of $HO^{\cdot}$ radicals for photodegredation pathway. In addition, scavengers study showed the role of electrons, holes, superoxides and $HO^{\cdot}$ radicals. Besides, reusability study for the different organic dyes using the titania@silica NCs indicated that we could obtain the photocatalyst after five successive cycles with high reactivity.

## 2 Experimental pathways

### 2.1 Materials

Ultra-high pure materials were obtained from Sigma Aldrich; including cetyltrimethylammonium bromide (CTAB), tetraethylorthosilicate (TEOS), ammonium hydroxide, absolute ethanol, titanium isopropoxide, isopropanol and glacial acetic acid. Furthermore, methylene blue, safranin and eosin used as organic dyes models for the pollutant degradation studies.

### 2.2 Synthesis of $SiO_2$ nanoparticles

Sol–gel route was used to design silica nanoparticles [31] using hydrolyzing of TEOS as silica precursor source in a solution mixture including ethyl alcohol, ammonia solution and CTAB. A 70 ml solution of TEOS and 10 ml of CTAB solution (1 gm of CTAB in 100 ml distillated water) stirred together for 1 h. Then, neutral point reached by adding of ammonia and checking the pH, the reaction solution still clear for some time. Then, after formation of silica gel, the solution become turbid and completed in 2 h. The final steps to obtain $SiO_2$ nanoparticles were drying for 2 days, followed by calcination process for 2 h at 640 °C.

### 2.3 Preparation of $TiO_2$ nanoparticles

Titania nanoparticles were synthesized as mentioned elsewhere [32]. 10 ml of titanium isopropoxide added and mixed to 100 ml isopropanol, and mixed together with constant stirring for 2 h. Then, appropriate amount (2 ml) of CTAB solution was pulled into the solution and continue stirred for 3 h. After that, distilled water was dropwise to this solution until turbid sol was obtained. Filtering, washing with distilled water are the following processes for the obtained sol to remove any salts and residues. After that, drying process for the gel occurred at 80 °C in dryer machine for 1 day to get rid of any moisture. Finally, calcination step of the final sample attained at 500 °C for 3 h to tear out CTAB and induce crystallization of titania nanoparticles.

### 2.4 Synthesis of $TiO_2$@$SiO_2$ nanocomposites

An appropriate amount ratio (1:1 wt%) of titania and silica were mixed together in isopropanol solution and stirred for 1 h to get five wt% titania over silica. 5 gm of CTAB in acetic acid was mixed to the above solution and stirred for 2 h. Then, the gel formed after 48 h, which filtered and washed many times with distilled water to get rid of any impurities. Finally, the sample was annealed at 600 °C for 3 h to get the titania@silica NCs final form.

### 2.5 Characterization of the obtained materials

The techniques used for measurement and characterization of the obtained materials including XRD, BET surface area, FESEM, HR-TEM, UV–Vis-NIR spectrophotometer and the photoluminescence (PL) spectra were detected using the same machines as mentioned in our previous studies [33, 34].

### 2.6 Photocatalytic activity tests

The maximum absorption peak of degradation of MB, safranine and eosin investigated at 254 nm using UV-C mercury lamp. The absorption peaks of used dyes were indicated at wavelength equal to 664, 518 and 520 nm for MB, eosin and safranin, respectively. Other studies were detect and confirm the methods steps of the degradation reaction through adsorption, photolysis and photocatalysis steps indicating the contribution of these conditions as well as the parameters used for this pathway which are the same in our current work [33, 35]. Besides, detection of point of zero charge (pzc) for the obtained samples attained through the detection of pH.

### 2.7 Chemical oxygen demand (COD)

The photo-degradation process used to measure and detect all organic compounds [36]. Furthermore, $CO_2$, $H_2O$ and electrons are the output product of organic compounds

oxidation, and the obtained electrons can reduce the oxidizing chemicals easily while the oxidation reaction occur.

## 3 Results and discussion

### 3.1 Structural investigation of $TiO_2$@$SiO_2$ nanocomposites

#### 3.1.1 Crystal structure characterization

The crystalline phase of the obtained materials was illustrated at Fig. 1. The X-ray powder diffraction pattern (XRD) of $SiO_2$, observed spectrum appears as a broad band with the equivalent Bragg angle at 2θ between 20 and 30°, which indicates that the material is amorphous with no certain crystalline peaks as shown in Fig. 1b (red line). Furthermore, XRD pattern, crystalline phase and size of titania were detected which shows different peaks at 23.3°, 38.9°, 43°, 55.1°, 62.6° and 68.7° which matched well to the titania anatase phase (JCPDS No. 71-1167 were a = 3.786 Å and c = 9.507 Å) as shown in (Fig. 1a, black line). Although silica shows amorphous phase, the obtained $TiO_2$@$SiO_2$ NCs samples illustrate a crystalline structure. It comes from the covering of titania on the surface of the silica as shown in Fig. 1c, blue line. Plainly, the small size of the $TiO_2$@$SiO_2$ NCs can easily confirmed through the broadening of XRD peaks obtained from the results. Titania@silica sample showed broad band of silica at the equivalent Bragg angle at 2θ between 20 and 30° and different peaks at 23.3°, 38.9°, 43°, 55.1°, 62.6° and 68.7° for titania anatase phase. Subsequently, the XRD patterns did not show any other phases for the obtained samples, confirming that the NCs structure was complete formed and in pure phase.

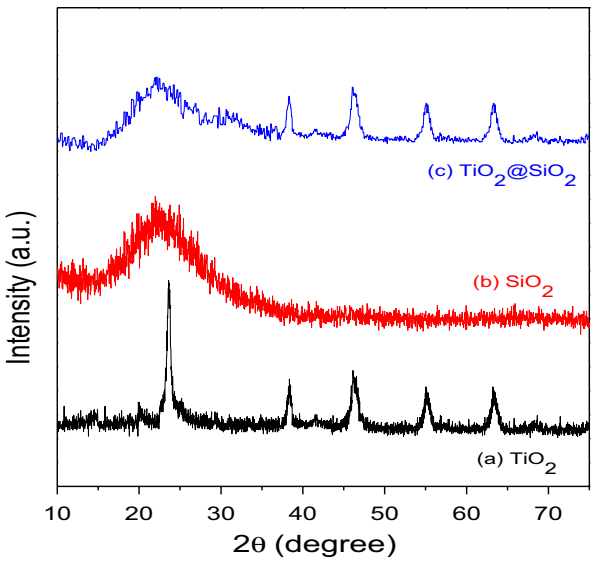


**Fig. 1** XRD patterns of $TiO_2$ (black line), $SiO_2$ (blue line) and $TiO_2$@$SiO_2$ (red line) nanomaterials (Color figure online)

#### 3.1.2 Textural and surface area characterization of samples

FESEM and TEM analysis were used to investigate the synthesized materials morphology. Figure 2a–c shows the FESEM results of $TiO_2$, $SiO_2$ nanoparticles as well as $TiO_2$@$SiO_2$ NCs materials, respectively. As revealed, $TiO_2$ is clearly possesses tiny sphere particles like morphology grown in high density and agglomerated in a homogeneous way as shown in Fig. 2a. Furthermore, Fig. 2b illustrates the structure of $SiO_2$ nanoparticles, which plainly related to the formation of bulky spherical nanoparticles, along with porous structure and tendency for agglomeration. In addition, the morphology of $TiO_2$@$SiO_2$ NCs was illustrated in Fig. 2c, in which its general morphology is dominated. The structure of the NCs is clearly identified that $TiO_2$ nanoparticles are dispersed above $SiO_2$ nanoparticles surface matrix. For more deep details for the morphology and structure of $TiO_2$@$SiO_2$, TEM analysis was studied. Different magnifications at 1 µm, 200 and 50 nm were undertaken to confirm the formation of the NCs structure. The obtained results exhibited homogeneous morphology and confirm the formation of bulky spherical nanoparticles for silica matrix surrounded and covered by dark titania nanoparticles in a uniform structure as shown in Fig. 2d, f. From the TEM images, it is clear that the formed $TiO_2$@$SiO_2$ NCs possessed crystalline characters. The as-prepared $TiO_2$ nanoparticles consists of spherical particles as illustrated in Fig. 2e. The mesoporous characteristics within nanoparticles indicating that $TiO_2$ nanoparticles has comparatively good stability during the preparation process.

Furthermore, Fig. 3a illustrates the complete isotherms of $N_2$ adsorption of $SiO_2$ as well as $TiO_2$@$SiO_2$ samples at low temperature about 77 k to show the impact of $TiO_2$@$SiO_2$ NCs on the textural properties. The adsorption isotherm are exhibited ($H_2$) hysteresis loop that closes at relative pressure of 0.421 and 0.653 for $SiO_2$ and $TiO_2$@$SiO_2$ samples, respectively as shown in Fig. 3a. This type of hysteresis includes desorption behavior which different from adsorption due to capillary cracks. Furthermore, adsorption of titania over silica is affected the $N_2$ sorption characteristics of silica that appears to reflect the mode of interaction between silica and titania. The mechanism of spreading titania over silica can explained due to the existence of the active pores in the entire surface of silica which targeted by the titania particles to fill them. This result is dedicated through the change in C constant from 60.3 to 122.8 for $SiO_2$ and $TiO_2$@$SiO_2$, respectively. Moreover, another confirmation of this phenomenon comes from the decrease in surface polarity

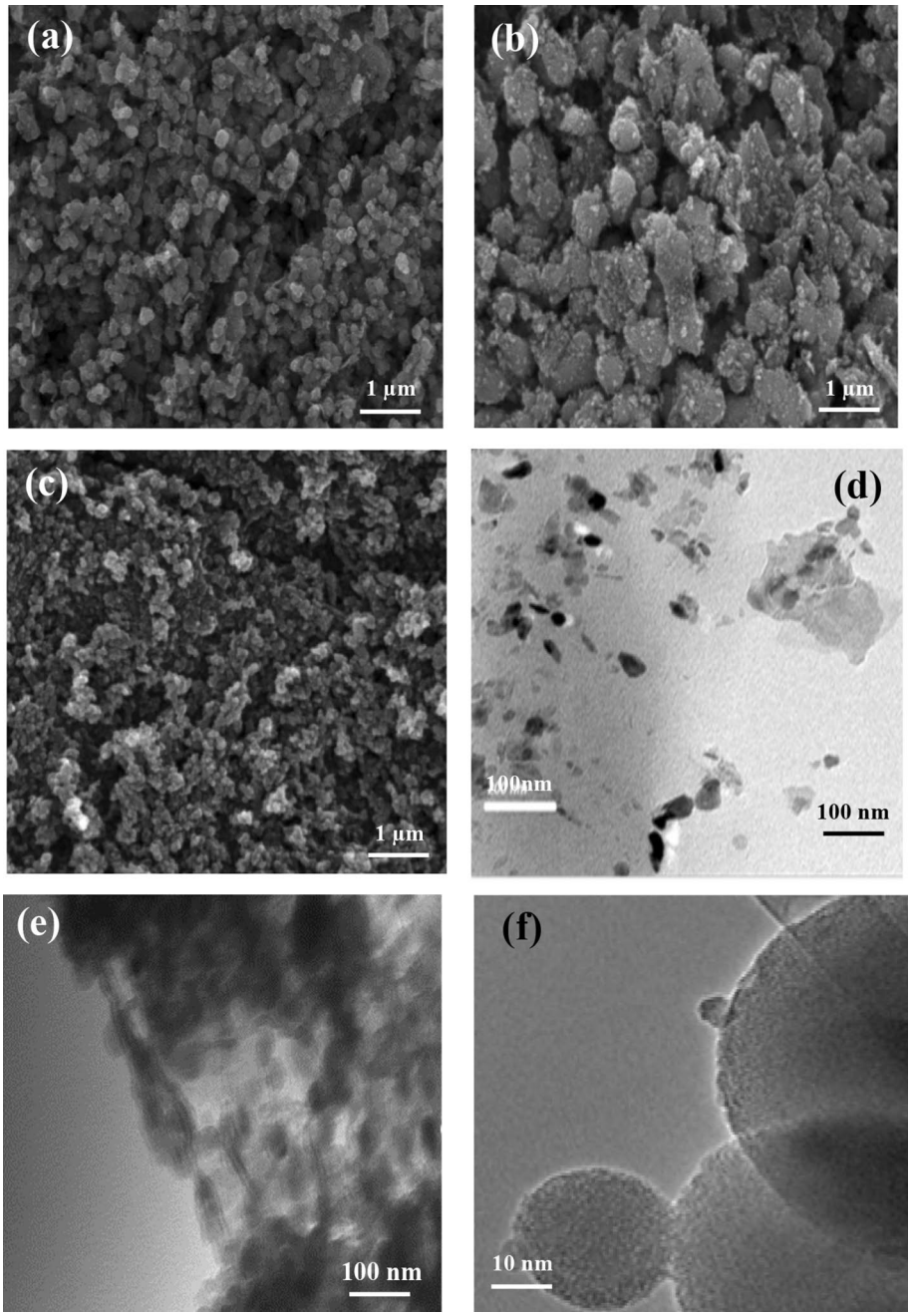


**Fig. 2** FESEM images of **a** $TiO_2$, **b** $SiO_2$ and **c** $TiO_2$@$SiO_2$, respectively; **d**, **e** TEM of TiO2 and $TiO_2$@$SiO_2$ and **f** HRTEM of $TiO_2$@$SiO_2$ nanocomposite materials

after spreading of titania samples over silica. In addition, specific surface area, total pore volume and average pore radius results of $SiO_2$ and $TiO_2$@$SiO_2$ samples were shown in Table 1.

Porosity manipulation was skilled by illustrating V–t plot measurement. Figure 3b shows the t-curve for pure $SiO_2$ as well as $TiO_2$@$SiO_2$ NCs and showed downward and upward deviation for $SiO_2$ and $TiO_2$@$SiO_2$. Surface area and pore volume values show critical decrease, while pore radius indicates noticeable increase from the surface parameters results obtained. The reason behind these behaviors was the change of some microspores structure to mesoporous due to deposition of titania inside some pores, the pore size distributions of the powders were represented in Fig. 3b (inset). It is plainly showed that a narrow curve in pure silica confirms that all the size of samples pores were almost the same. However, the results refers to existence of two peaks from spreading of titania over silica, the first one is located at 20 Å which refers to supermicropores, while the second broad one is founded at 31 Å shows a wide spectrum of sample mesoporosity [37].

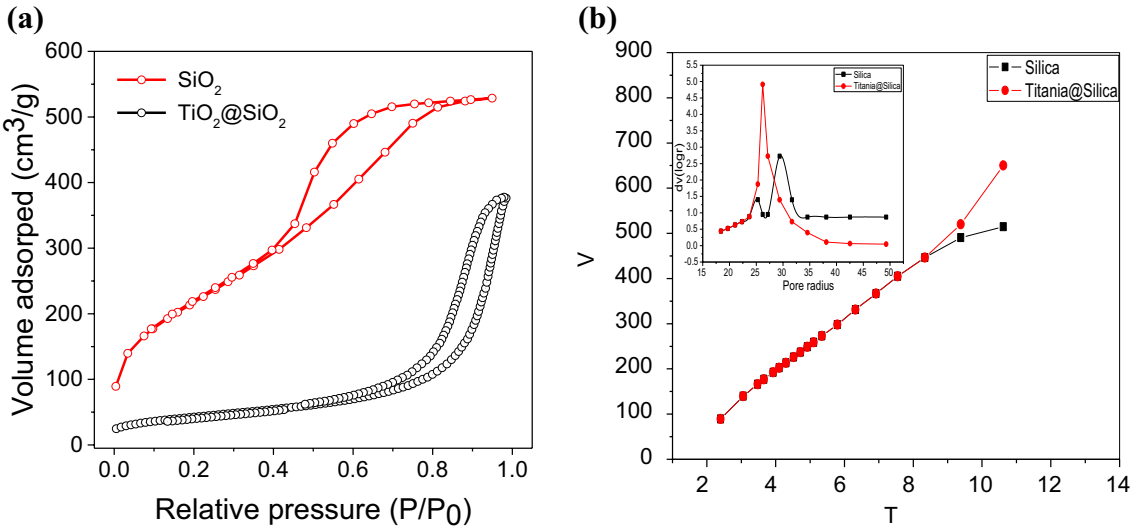


**Fig. 3** **a** $N_2$ adsorption–desorption isotherms surface area and **b** corresponding pore size distribution as well as V–t plot of $SiO_2$ and $TiO_2$@$SiO_2$

**Table 1** Physical properties of $SiO_2$ nanoparticles and $TiO_2$@$SiO_2$ nanocomposite

| Sample | $S_{BET}$ ($m^2\ g^{-1}$) | Pore volume ($cm^3\ g^{-1}$) | Average pore size (nm) | Porosity (%) | BJH adsorption (nm) | BJH desorption (nm) |
|---|---|---|---|---|---|---|
| $SiO_2$ | 765.85 | 0.632 | 20.1 | 51 | 20 | 16 |
| $TiO_2/SiO_2$ | 140.5 | 0.214 | 29.4 | 92 | 31 | 23 |

### 3.2 Optical properties and photoluminescence spectra

Band gap energy ($E_g$) relays on the delocalization of orbitals at specific wavelengths of the prepared nanoparticles materials. Silica ($SiO_2$) has very wide $E_g$ which considered the main problem which restricts the photo reactivity; while, titania has $E_g$ of (3.2 eV) which lie in the ultraviolet region. Coating titania over silica surface reducing the $E_g$ to lower value (−3.0 eV) which makes the photo-excitation of it more adapted and respond to the ultraviolet region. The absorbance spectra of $TiO_2$, $TiO_2$@$SiO_2$ is displayed in Fig. 4a and confirm the formation of a very sharp band edge in the UV region at 200–300 nm for $TiO_2$, from 300 to 400 nm for $TiO_2$@$SiO_2$. On careful examining, it can notice that $TiO_2$@$SiO_2$ NCs sample exhibit a red shift to higher wavelength indicating a favorable absorbance toward visible light. In addition, $E_g$ for $TiO_2$ as well as $TiO_2$@$SiO_2$ is measured through the relation between absorbance coefficient $(\alpha hv)^2$ and energy (E) as illustrated in Fig. 4b. Subsequently, in order to predict the reason behind the improvement in photocatalytic performance of designed NCs structures, PL spectra was measured. From the obtained results, the degradation of the examined organic dyes was enhanced because of the efficient separation of photo-generated electron-hole pairs in $TiO_2$ as well as $SiO_2$ of $TiO_2$@$SiO_2$ NCs systems. Figure 4c illustrates the existence of one peak at wavelength of 415 nm, which related to the defects in $TiO_2$. From the results obtained, a strong quenching can be noticed due to the covering of $TiO_2$ nanoparticles above $SiO_2$ sample. The good contact between titania and silica in the $TiO_2$@$SiO_2$ NCs network as well as the lower recombination rate of mixed oxides may be the possible reasons behind the quenching occurred and affect positively on removing and degradation of the pollutant easily from the organic dyes [38].

### 3.3 Photocatalytic degradation of organic dyes

Novel and easy prepared $SiO_2$ and $TiO_2$@$SiO_2$ NCs materials have been conducted for photodegradation of different dyes. Photocatalytic activities of these materials were dedicated by get rid of safranin, MB as cationic and eosin as anionic dyes model with molar concentration ($2\times10^{-5}$mol/l) under UV irradiation where MB, eosin and safranin show absorption spectra peaks at 664, 518 and 520 nm wavelengths, respectively, with the about 120 min irradiation time as shown in Fig. 5. The decoloration of different organic dyes used in this study could be explained by the oxidative dyes photodegradation [39], the photocatalytic

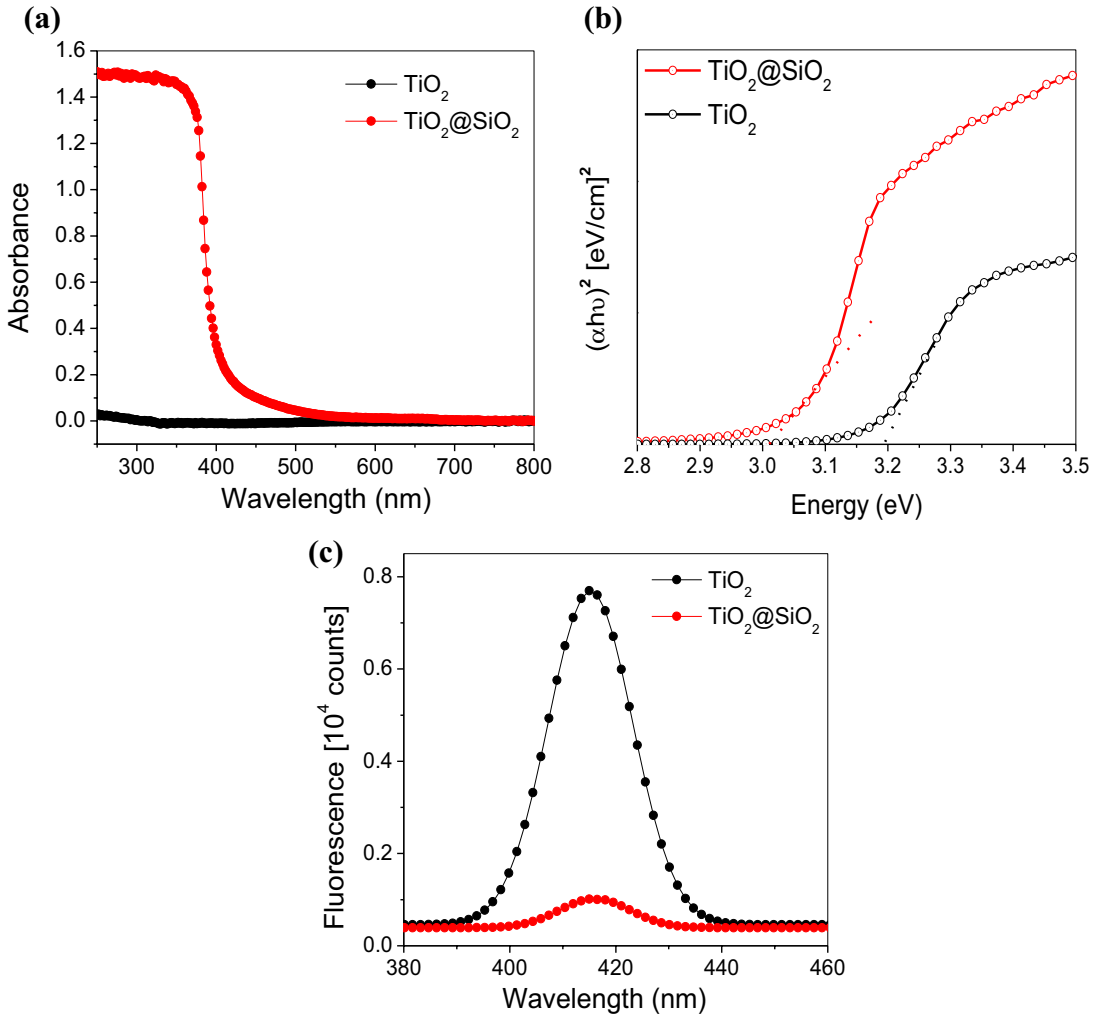


**Fig. 4** **a** Absorption spectra, **b** band gap energy and **c** photoluminescence (PL) spectra of $SiO_2$ nanoparticles and $TiO_2$@$SiO_2$ nanocomposite, respectively

performance was significantly improved with $TiO_2$@$SiO_2$ NCs. Figures 5a–f shows the absorption spectra and the photocatalytic degradation process of MB, eosin and safranin dyes by using $TiO_2$ and $TiO_2$@$SiO_2$ materials, respectively. Furthermore, photodegredation process of the safranine, as an example for the different organic dyes used in this study, obeys pseudo first order kinetics as shown in Fig. 6. The rate constant for the reaction calculated from the relation between ln $C_o$/C and contact time, and the linear behavior of ln $C_o$/C and time shows the degradation process follows the pseudo first order reaction behavior. By applying the same behavior, we surmised that the response of the other used organic dyes for the pollutant degradation should be the same by using different $TiO_2$, $SiO_2$ and $TiO_2$@$SiO_2$ semiconductors. Blank test [organic dye solution (safranin, MB, eosin) without any photocatalyst] shows that any of the organic dyes exhibit less than 5% photolysis. No doubt that, addendum of $TiO_2$@$SiO_2$ could enhance the photocatalytic execution of the NCs. In addition, 120 min of illumination reaction explains the highly efficient behavior of obtained photocatalyst towards removal of dye molecules. Furthermore, about 32% and 5% of the safranin or MB dyes used was degraded for pure silica that decrease with increasing the doping of titania above silica surface, and about 1.25% of eosin is degraded via dark reaction confirming the complete destruction of the pollutant into inorganic molecules proceeded through the removal process. From the results obtained, the removal percentage of dyes increases with increasing spreading titania over the surface of silica due to filling of all pores with increasing of doping ratio. This behavior obtained through the charge separation mechanism which facilitate the generation of oxidizing species like $HO^{\cdot}$ radicals and $O_2^{\bullet-}$ radicals which are the main precursors for the destruction of target pollutant [40, 41]. Many reasons behind the enhanced photocatalytic activity of $TiO_2$@$SiO_2$

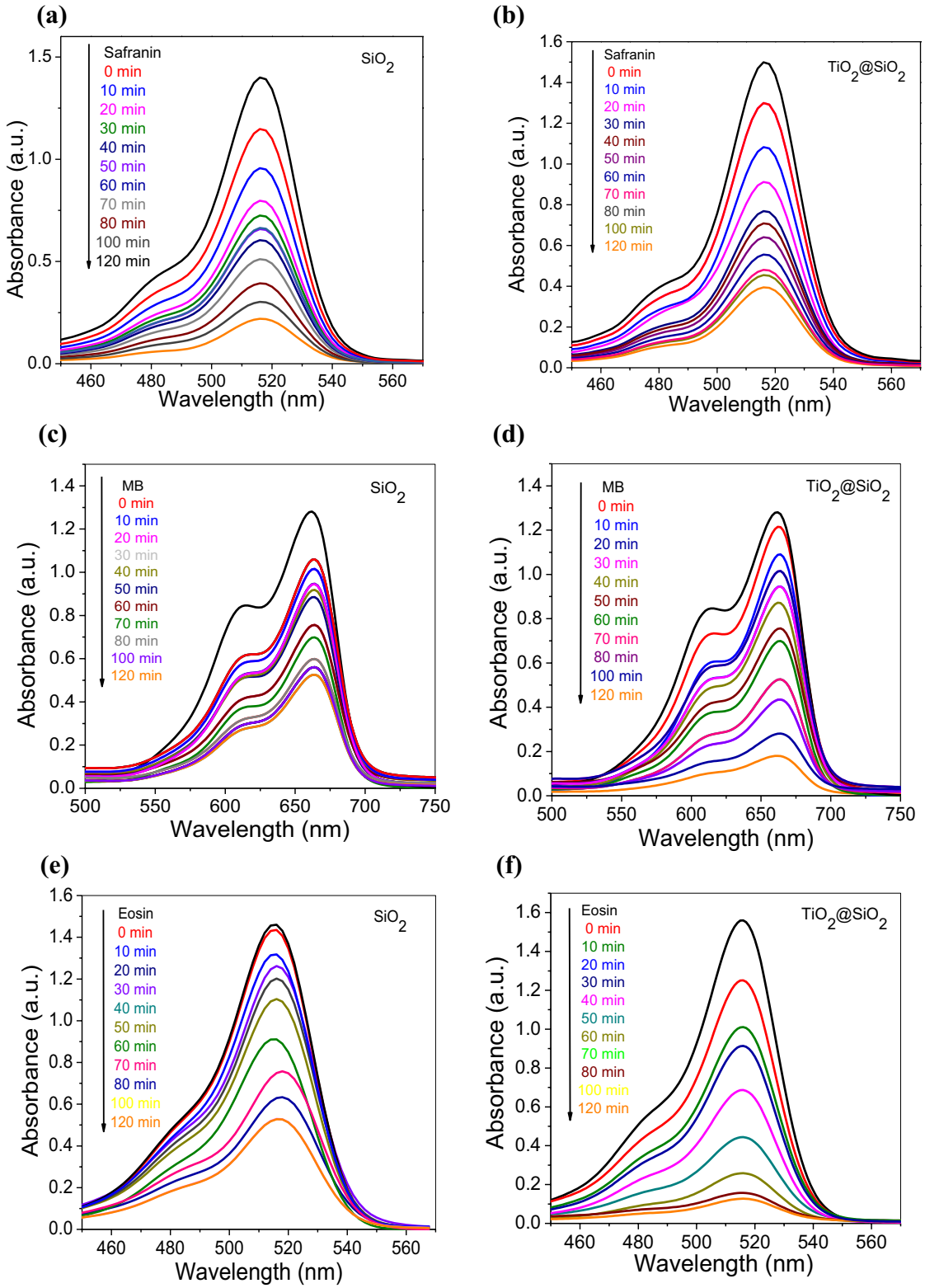


**Fig. 5** Absorption spectra of photocatalytic degradation of (**a**, **b**) safranine, (**c**, **d**) MB and (**e**, **f**) eosin dyes over $SiO_2$ and $TiO_2$@$SiO_2$, respectively

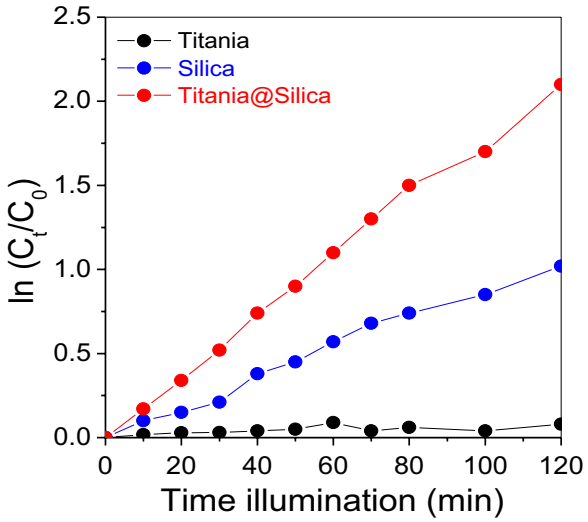


**Fig. 6** The pseudo first order kinetics of degradation of safranin as example for the organic dyes in this study using different $TiO_2$, $SiO_2$ and $TiO_2$@$SiO_2$ semiconductors for the pollutant degradation

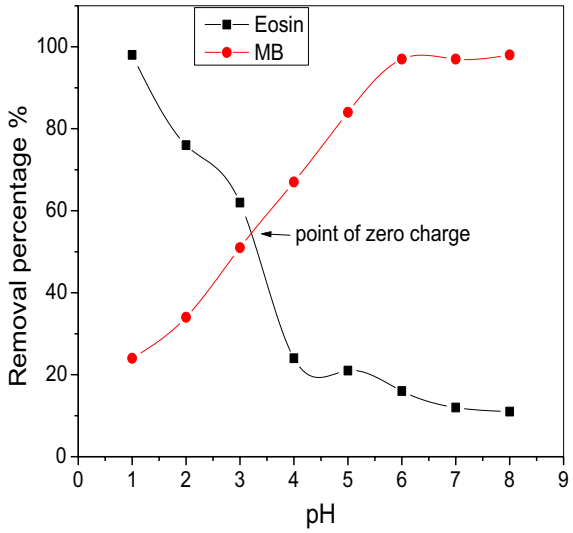


**Fig. 7** The relation between pH values and the removal percentage of different organic dye (eosin and methylene blue) dyes in presence of $TiO_2$@$SiO_2$ nanocomposites for the pollutant degradation

NCs like its high surface area, pore volume and low band gap which facilitate the pollutant removal easily.

### 3.4 Factors influence photodegradation process

Removal of toxic organic pollutant founded in water is the main target of the active photocatalyst materials under UV irradiation. We speculate, when the light irradiated to these materials, electrons and holes pairs were generated and facilitate the degradation of the organic residues into inorganic ones. Ease assembled and low cost titania@silica NCs are considered as a promising photocatalyst to get rid of organic residues. It is noticed that the increment of photocatalyst loading can increase the dye removal %. Furthermore, homogeneous distribution of titania nanoparticles on silica surface can enhance the photocatalytic properties to the optimum. With increasing the weight, the photoactivity decreased [42, 43]. Sometimes, it is considered that few agglomerations of $TiO_2$ nanoparticles can occur on the surface of $SiO_2$ particles at high concentration and the number of surface active sites decreases, which inhibited the photocatalytic activity due to the increase in the opacity, and light scattering of the photocatalyst. The relation between the dye removal percentage and the pH is speculated being directly proportional, as the pH value increase the dye removal percentage increase until the isoelectric point at which the charge of the surface becomes negative, and the surface of the metal will exhibit repulsive behavior with the dye after this limit. This phenomenon can confirm that, dyes have negative charge, whereas $TiO_2$@$SiO_2$ has positive charge in acidic medium under pH of three [44]. Furthermore, the relation between pH values and the removal percentage of different organic dye (eosin and MB) dyes in presence of $TiO_2$@$SiO_2$ NCs for the pollutant degradation is illustrated in Fig. 7. In addition, the time of dye degradation is also an important factor, which controls the photocatalyst activity. The $TiO_2$@$SiO_2$ photocatalyst have active sites to carry out the reaction and the degradation of the pollutant occurs in such short time, which makes it a good candidate for organic pollutant removal. In this work, we do different experiments like changing concentration of dye, concentration of photocatalyst, doping ratios, pH, and weight of the precursor as well as method of doping to check the optimum conditions for obtaining good photocatalysts for dye pollutant removal.

### 3.5 Detection of HO˙ radicals using effect of terephthalic acid

The photolysis of terephthalic acid through the PL probing technique confirms the existence of HO˙ radicals. Although, terephthalic acid is non-fluorescent, the fluorescent behavior come from the connection with HO˙ obtained from the $TiO_2$@$SiO_2$ NCs to obtain 2-hydroxy terephthalic acid. The obtained results confirms that there is no peaks given to terephthalic acid, while for $TiO_2$@$SiO_2$ peaks founded at 420 nm confirming the presence of HO˙ radicals and fluorescence intensity increases with increasing contact time as Fig. 8 illustrated.

### 3.6 Calculation of the chemical oxygen demand (COD)

Pollutant degradation can be measured from the amount of oxygen needed for the oxidation of organic constituents

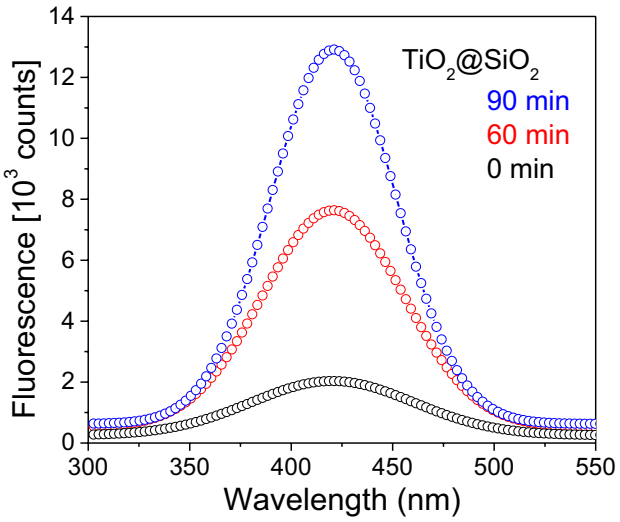


**Fig. 8** $HO^{\cdot}$ trapping photoluminescence spectral changes observed during irradiation of $TiO_2$@$SiO_2$ nanocomposite (15) % in a $5\times10^{-4}$ M terephthalic acid solution (excitation at 315 nm)

using COD tests [45]. It is noticed that COD reduces analytically from 21.6 ppm before the photo catalytic process to 1.2 ppm after 90 min of irradiation by UV on $TiO_2$@$SiO_2$ for any of the three dyes used in this study. The obtained chemical oxygen demand results are confirming the removal results showing the complete degradation of organic components.

### 3.7 pH effect on the photodegradation of organic dye pollutants

Point of zero charge determination is found to be 2.5 and 3.2 for $SiO_2$ and $TiO_2$@$SiO_2$, respectively. The working conditions of the materials determination were at pH 7 which higher than the pzc and make the surface anionic. This explains the observed adsorption of safranine or MB as cationic model over the surface of silica nanoparticles. Efficiency of photodegredation of safranine or MB dyes is maximum near the pzc (pH 3.2). The results obtained indicated that the change in pH either at low or high values refers to the same results obtained for our previous NCs photocatalysis [33]. Consequently, the existence of hydroxyl groups at high pH can increase the absorbability of cationic and anionic model dyes on the surface of $TiO_2$@$SiO_2$ NCs photocatalysis through hydrogen bonding [46]. The results indicated that, the optimum pH value for the photodegradation of eosin dye is ~ 3.2 at which photocatalytic oxidation is being maximum.

### 3.8 Radical scavenger's effect

Different scavengers have been conducted for the detection of the major active species responsible for the photodegradation process through different experiments as shown in Fig. 9a. Different scavengers like KI, isopropanol, silver nitrate and benzoquinone were used on the surface of $TiO_2$@$SiO_2$ NCs. Typically, experiments were carried out under the same reaction parameters like previous work indicated [33, 47, 48]. There is no noticable effect in dye photodegradation

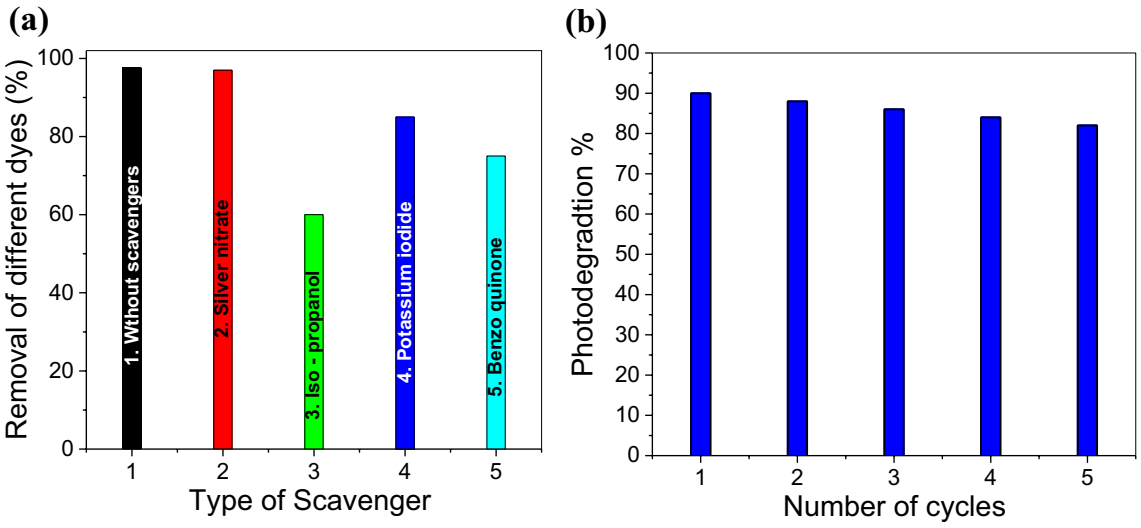


**Fig. 9** **a** The effect of various scavengers over $TiO_2$@$SiO_2$, **b** regeneration of $TiO_2$@$SiO_2$ nanocomposites for five successive cycles for the MB dye used in this study

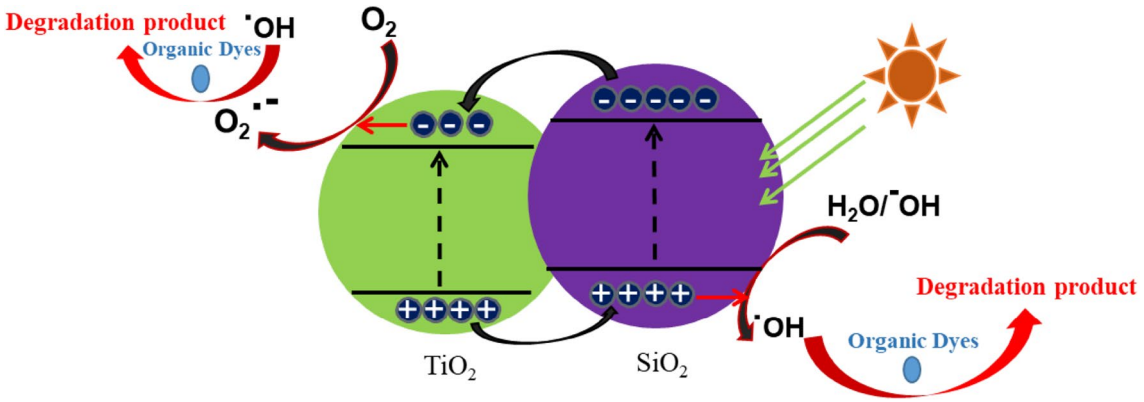


**Scheme 1** Schematic illustration of the proposed mechanism of the charge separation, absorption of UV light by the $SiO_2$ promotes an electron from the valence band to the conduction band. This produces electron–hole pairs, which generates oxidatives species such as $O_2^{\bullet-}$and OH to undergo further reactions and enhance photocatalytic activity of mesoporous $TiO_2$@$SiO_2$ nanocomposites for photodegradation of three different organic dyes (eosin, MB and safranine) pollutant

in the presence of silver nitrate and benzoquinone, confirming that the negative electrons ($e^-$), positive hole ($h^+$) and superoxide ($O_2^{\cdot-}$) are the minor active species acting in the photocatalytic reaction. However, a major effect on the photocatalytic event was observed upon the addition of isopropanol (scavenger for $HO^{\cdot}$), which confirms that the $HO^{\cdot}$ species are the main photoactive species participating in the degradation process. In another words, we can speculate that the $HO^{\cdot}$ species are responsible for the photocatalytic degradation process of different dyes used in this study over titania@silica NCs [48].

### 3.9 Photocatalytic mechanism

Many factors can control the enhancement of photocatalysts as mentioned elsewhere [49]. From the discussed results in this study, a photo-reaction mechanism is explained as mention below: $TiO_2$@$SiO_2$ NCs could create oxidizing species, which responsible for different dyes degradation in this study. Charge separation happened at the HOMO and LUMO of the nanocomposite photocatalysis materials owing to its $\pi$–$\pi^*$ moves characteristic [50, 51]. Furthermore, $TiO_2$ and $SiO_2$ are matching together in a good manner, enabling the charge ($e^-$ and $h^+$) separation and transfer easily between each other. The ease transfer of holes from $TiO_2$ to $SiO_2$ when $TiO_2$@$SiO_2$ NCs irradiated with light is coming from the difference between the VB edge potential of both materials, as it's lower in $TiO_2$ than of $SiO_2$. While, the electron transfers from the CB of $SiO_2$ to CB of $TiO_2$. The transferred holes can react with $H_2O$ to produce hydroxyl radicals ($HO^{\cdot}$) which facilitate photocatalytic oxidation process, while the electrons reducing $O_2$–$O_2^{\cdot-}$ (as shown in Scheme 1) [52, 53]. Besides that, the charge separation enhanced and the recombination restrained due to the possible excitation of $TiO_2$ besides $SiO_2$ to get $TiO_2$@$SiO_2$ NCs.

### 3.10 Reusability of the obtained photocatalyst

It is well known that photocatalyst reusability is critical to determine the obtained samples; and it must have retain its reactivity after each reaction cycle. The photoactive stability of $TiO_2$@$SiO_2$ NCs photocatalyst was detected and evaluated for different dyes used in this study after five successive cycles by recycled experiments. Minimal loss in the degradation rate can be confirmed after five cycles of catalytic activity by using the $TiO_2$@$SiO_2$ photocatalyst as illustrated in Fig. 9b. It is plainly noticed that the photo catalyst maintains 60% of its reactivity after the five cycles indicating the high stability of the $TiO_2$@$SiO_2$ composite catalyst upon exposure to light. Furthermore, the slight decrease in photocatalytic activity may be come from loss of photocatalyst during washing and separation.

## 4 Conclusion

A simple chemical method was performed to synthesize $TiO_2$@$SiO_2$ nanocomposite photocatalysts with high efficiency for pollutant degradation. The products were checked using XRD, BET, FESEM, TEM, PL, UV–Vis spectroscopy and zeta potential analysis. XRD analysis confirmed the presence of anatase phase of $TiO_2$ and a plain structure of $TiO_2$@$SiO_2$ NCs without any impurities. The titania@silica NCs indicated better photocatalytic performance for eosin, safranin and MB dyes degradation under ultra violet light illumination, which was much higher than that of pure $SiO_2$ nanoparticles. The enhancement in charge separation between the $SiO_2$ and $TiO_2$ comes from the activity enhancement of $TiO_2$@$SiO_2$ photocatalysis NCs. The enhanced photocatalytic activity

and low preparation cost suggest the practical implementation of this promising materials for use in environmental remediation, solar cells, related nano devices, and other applications.

**Acknowledgments** British University in Egypt is appreciated by the authors for its assistance to follow up this study. Furthermore, the technical service units of Central Laboratory, Cairo University as well as CMRDI are also gratefully gratitude.

**Funding** No contending financial interest proclaim by the authors.

## References

1. K.O. Badmus, J.O. Tijani, E. Massima, L. Petrik, Environ. Sci. Pollut. Res. **25**, 7299–7314 (2018)
2. C. Salvador, L. Javier, C. Pablo, C. Davide, C. Giacomo, A.R. Manuel, P. Marco, Electrochim. Acta **263**, 1–7 (2018)
3. H. Hamad, D. Bassyouni, E.S. El-Ashtoukhy, N. Amin, M.A. El-Latif, Ecotoxicol. Environ. Saf. **148**, 501–512 (2018)
4. H. Wang, L. Zhang, C. Hu, X. Wang, L. Lyu, G. Sheng, Chem. Eng. J. **332**, 572–581 (2018)
5. A.Y. Zhang, Y.Y. He, Y.P. Chen, J.W. Feng, N.H. Huang, F. Lian, Chem. Eng. J. **334**, 1430–1439 (2018)
6. A.A. Attia, B.S. Girgis, N.A. Fathy, Dyes Pigm. **76**, 282–289 (2008)
7. C. Montserrat, A.M. Carmen, R. Josep, B. Damià, Environ. Sci. Technol. **33**, 1300–1306 (1999)
8. M.M. Rashad, A.E. Shalan, J. Mater. Sci. Mater. Electron. **24**, 3189–3194 (2013)
9. D. Farrusseng, S. Aguado, C. Pinel, Angew. Chem. Int. Ed. **48**, 7502–7513 (2009)
10. P.K. Malik, Dyes Pigm. **56**, 239–249 (2003)
11. K.V. Oomman, G. Dawei, P. Maggie, A.G. Craig, C.D. Elizabeth, J. Mater. Res. **18**, 156–165 (2003)
12. T. Ohno, T. Mitsui, M. Matsumura, Chem. Lett. **32**, 364–365 (2003)
13. I. Sopyan, M. Watanabe, S. Murasaw, K. Hashimoto, A. Fujishim, J. Electroanal. Chem. **415**, 183–186 (1996)
14. M.M. Rashad, A.E. Shalan, Appl. Phys. A **116**, 781–788 (2014)
15. G.S. Cláudia, J. Raquel, M. Tiziana, M. Raffaele, G. Hermenegildo, J. Am. Chem. Soc. **133**, 595–602 (2010)
16. A.L. Linsebigler, G. Lu, J.R. Yates, Chem. Rev. **95**, 735–758 (1995)
17. A.E. Shalan, A.M. Elseman, M. Rasly, M.M. Moharam, M. Lira-Cantu, M.M. Rashad, RSC Adv. **5**, 103095–103104 (2015)
18. V. Mahmoodi, T.R. Bastami, A. Ahmadpour, Environ. Sci. Pollut. Res. **25**, 1–18 (2018)
19. A. Mills, C. O'Rourke, K. Moore, J. Photochem. Photobiol. A Chem. **310**, 66–105 (2015)
20. B. Srikanth, R. Goutham, N.R. Badri, A. Ramprasath, K.P. Gopinath, A.R. Sankaranarayanan, J. Environ. Manage. **200**, 60–78 (2017)
21. A. Roberto, C. Vincenzo, I. Amedeo, M. Raffaele, Catal. Today **53**, 51–59 (1999)
22. P.V. Kamat, D. Meisel, Curr. Opin. Colloid Interface Sci. **7**, 282–287 (2002)
23. C. Galindo, P. Jacques, A. Kalt, J. Photochem. Photobiol. A Chem. **130**, 35–47 (2000)
24. M.M. Mohamed, W.A. Bayoumy, M. Khairy, M.A. Mousa, Microporous Mesoporous Mater. **103**, 174–183 (2007)
25. C.Y. Jimmy, Y. Jiaguo, Z. Lizhi, H. Wingkei, J. Photochem. Photobiol. A Chem. **148**, 263–271 (2002)
26. R.S. Mane, O.S. Joo, W.J. Lee, S.H. Han, Micron **38**, 85–90 (2007)
27. F.S. Francisco, B. Juan, C. Le, C. Peter, W. Mingkui, M.Z. Shaik, G. Michael, J. Am. Chem. Soc. **131**, 558–562 (2008)
28. A.E. Shalan, T. Oshikiri, S. Narra, M.M. Elshanawany, K. Ueno, H.P. Wu, K. Nakamura, X. Shi, E.W.G. Diau, H. Misawa, ACS Appl. Mater. Interfaces **8**, 33592–33600 (2016)
29. A.E. Shalan, M. Rasly, I. Osama, M.M. Rashad, I.A. Ibrahim, Ceram. Int. **40**, 11619–11626 (2014)
30. M.M.S. Sanad, A.E. Shalan, M.M. Rashad, M.H.H. Mahmoud, Appl. Surf. Sci. **359**, 315–322 (2015)
31. K.S. Rao, K. El-Hami, T. Kodaki, K. Matsushige, K. Makino, J. Colloid Interface Sci. **289**, 125–131 (2005)
32. A.E. Shalan, M.M. Rashad, Y. Yu, M. Lira-Cantú, M.S.A. Abdel-Mottaleb, Electrochim. Acta **89**, 469–478 (2013)
33. M.F. Sanad, A.E. Shalan, S.M. Bazid, S.M. Abdelbasir, J. Environ. Chem. Eng. **6**, 3981–3990 (2018)
34. M.M. Rahman, A. Jamal, S.B. Khan, M. Faisal, J. Nanopart. Res. **13**, 3789–3799 (2011)
35. M.M. Rashad, E.M. Elsayed, M.S. Al-Kotb, A.E. Shalan, J. Alloys Compd. **581**, 71–78 (2013)
36. A.M. Jirka, M.J. Carter, Anal. Chem. **47**, 1397–1402 (1975)
37. B. Ji, J. Zhang, C. Zhang, N. Li, T. Zhao, F. Chen, L. Hu, S. Zhang, Z. Wang, ACS Appl. Nano Mater. **1**, 793–799 (2018)
38. X. Deng, H. Zhang, Q. Ma, Y. Cui, X. Cheng, X. Li, M. Xie, Q. Cheng, Sep. Purif. Technol. **186**, 1–9 (2017)
39. R. Fateh, A.A. Ismail, R. Dillert, D.W. Bahnemann, J. Phys. Chem. C **115**, 10405–10411 (2011)
40. B. Sun, G. Zhou, T. Gao, H. Zhang, H. Yu, Appl. Surf. Sci. **364**, 322–331 (2016)
41. Y. Ku, C.N. Lin, W.M. Hou, J. Mol. Catal. A Chem. **349**, 20–27 (2011)
42. D. Chen, A.K. Ray, Water Res. **32**, 3223 (1998)
43. A. Mills, S. Morris, J. Photobiol. A Chem. **71**, 75 (1993)
44. C.A. Le Duc, J.M. Campbell, J.A. Rossin, Ind. Eng. Chem. Res. **35**, 2473 (1996)
45. S.H. Wu, D.H. Chen, J. Colloid Interface Sci. **273**, 165–169 (2004)
46. Z.M. El-Bahy, A.A. Ismail, R.M. Mohamed, J. Hazard. Mater. **166**, 138–143 (2009)
47. A. Helal, F.A. Harraz, A.A. Ismail, T.M. Sami, I.A. Ibrahim, Appl. Catal. B Environ. **213**, 18–27 (2017)
48. M. Faisal, F.A. Harraz, A.A. Ismail, A.M. El-Toni, S.A. Al-Sayari, A. Al-Hajry, M.S. Al-Assiri, Sep. Purif. Technol. **190**, 33–44 (2018)
49. L. Zhang, Y. Li, Q. Zhang, H. Wang, Cryst. Eng. Commun. **15**, 5986–5993 (2013)
50. K.R. Reddy, K.V. Karthik, S.B.B. Prasad, S.K. Soni, H.M. Jeong, A.V. Raghu, Polyhedron **120**, 169–174 (2016)
51. T. Zheng, J. Xu, Z. Zhang, H. Zeng, RSC Adv. **5**, 99658–99663 (2015)
52. A.A. Ismail, D.W. Bahnemann, J. Mater. Chem. **21**, 11686–11707 (2011)
53. C.X. Feng, S.Z. Wang, B.Y. Geng, Nanoscale **3**, 3695–3699 (2011)